

# Can Propagation of Gas Bubbles Lead to Detached Solidification? Experiments on Freezing of Water

Yazhen Wang,<sup>†</sup> Liya L. Regel,\* and William R. Wilcox\*

*International Center for Gravity Materials Science and Applications, Clarkson University, Potsdam, New York 13699-5814*

*Received February 1, 2002; Revised Manuscript Received June 10, 2002*

**ABSTRACT:** A vertical Bridgman-Stockbarger apparatus was used to directionally solidify water upward, in the hope that detached solidification would evolve from gas bubbles forming on the wall. A large contact angle of the water on the ampoule wall and a high solubility of the dissolved gas caused gas bubbles or tubes to form only at the ampoule wall, and not in the interior. Gas tubes were often nearly periodically spaced around the ampoule wall, with a spacing that increased with ampoule diameter and decreased with freezing rate. The width of the gas tubes was nearly independent of the ampoule diameter and freezing rate. A high degree of detachment was obtained with a rough, nonwetting coating on the ampoule wall, but full detachment was not achieved. This indicates that detachment does not occur by propagation of a single gas bubble around the periphery of the freezing interface. The convection near the freezing interface influenced gas bubble formation, and was outward for a concave freezing interface and inward for a convex interface.

## 1. Introduction and Background

Directional solidification in microgravity has frequently given rise to solids that grew without complete contact with the ampoule wall (see, for example, ref 1). Some success has been achieved in attaining such detached solidification on earth.<sup>2–9</sup> Steady-state detached growth was explained by the moving meniscus model.<sup>10–19</sup> However, the mechanisms by which detachment begins have not been fully explored. One method is to use a seed smaller in diameter than the ampoule, fill the gap with an inert gas, and take care not to completely melt back the seed prior to solidification.<sup>2,3</sup> In the vast majority of experiments, detachment occurred spontaneously in opaque furnaces, and initiation could not be observed. We have proposed two possible mechanisms for spontaneous initiation.<sup>10</sup> In one, the solid is initially in contact with the ampoule wall. When the coefficient of thermal expansion is larger for the solid than for the ampoule material, a stress builds up between the solid and the ampoule as they cool from the melting point. When this stress becomes sufficiently large to overcome adhesion, the solid pops free of the wall. If a dissolved gas has become concentrated at the freezing interface because of segregation, this gas is liberated into the gap suddenly formed between the solid and the wall. Filling the gap with a gas maintains the required pressure difference across the meniscus connecting the edge of the freezing interface with the ampoule wall.

Another proposed mechanism for initiation of detachment involves forming a gas bubble at the wall that subsequently propagates around the periphery of the freezing interface. (Detachment can be regarded as a

gas bubble completely surrounding the growing solid.) Here, we report on experiments performed to test this proposed mechanism. Water was chosen as an experimental medium primarily because it is low melting and transparent, permitting easy observation of bubble initiation and evolution, as well as convection in the melt adjacent to the freezing interface. Similar, but less extensive, experiments were performed using an organic compound, naphthalene.<sup>20</sup>

The formation and behavior of gas bubbles at a freezing interface can be explained in terms of the dissolved-gas concentration profile.<sup>21</sup> Gases are usually, if not always, more soluble in a melt than in the corresponding solid. Consequently, solidification causes the concentration of a dissolved gas to increase in the liquid adjacent to the growing crystal, as for any solute with a segregation coefficient  $< 1$ . When the impurity concentration becomes sufficiently high, a gas bubble may nucleate and grow. For example, Carte<sup>22</sup> observed directional freezing of thin layers of water. By application of the segregation equation for convectionless directional freezing, he estimated that a supersaturation of about 27 was required to nucleate air bubbles at the freezing interface.

After gas bubbles form, they may either float away or remain at the freezing interface, where they may be trapped in the solid as discrete bubbles, as chains of bubbles, or as gas tubes. The interaction of bubbles with the solidification interface determines which behavior is observed. For the water/ice system, Vasconcellos and Beech<sup>23</sup> observed that some bubbles at the freezing interface were trapped in the ice and some of them escaped. They claimed that if the buoyancy of a bubble is larger than its adhesive force to the interface, the bubble departs and rises to the surface of the melt. Cole et al.<sup>24</sup> developed a model for prediction of bubble departure radii from a flat freezing interface under both normal gravity and microgravity conditions in the presence of thermocapillarity (Marangoni effect). Bagda-

\* To whom correspondence should be addressed. Liya L. Regel, Clarkson University, Potsdam, NY 13699-5814. Phone: 1-315-268-7672, fax: 1-315-268-3833, E-mail: regel@clarkson.edu.

<sup>†</sup> Current address: Chemistry Department, Vanderbilt University, Nashville, TN 37235.

sarov et al.<sup>25</sup> showed by experiments and theoretical analysis that bubbles originally present in water were not captured by ice. Only the bubbles formed at the freezing interface were captured. Geguzin and Dzyuba<sup>26</sup> predicted that bubbles not on the interface would migrate in the direction of increasing temperature because of thermocapillarity.

Different shapes have been found for gas bubbles in solids. Maeno<sup>27</sup> concluded that the ratio of the growth rate of the bubble radius to the freezing rate is a major parameter determining the bubble shape in ice. When the growth rate of a bubble is larger it remains at the freezing interface where it absorbs more gas and becomes larger. When it is large enough, it escapes upward. When the growth rate is less than the freezing rate, it is captured. When the growth rate is comparable, the bubble forms a cylindrical gas tube in the ice.

Gas bubbles also occur during solidification of multi-component systems. For example,  $\text{CBr}_4\text{-C}_2\text{Cl}_6$  was directionally solidified in a thin film.<sup>28</sup> When constitutional supercooling caused the interface to become cellular, more segregated gas accumulated in the intercellular grooves. Bubbles nucleated in the grooves and grew until the bubble cap in the melt was ahead of the freezing interface.

Since bubble nucleation and growth depend on the concentration of dissolved gas near the freezing interface, we expect factors that influence this concentration to influence bubble behavior. For example, a higher concentration of dissolved gas in the melt prior to solidification should enhance bubble formation. For example, in 1845 many bubbles were trapped in ice when Brunner<sup>29</sup> froze water that had been boiled and cooled in air. He considered exposure to the air to be the reason for the formation of these bubbles. In 1870, Bunsen<sup>30</sup> obtained bubble-free ice by downward freezing of water that had been boiled in a tube that was subsequently sealed to exclude air. Vasconcellos and Beech<sup>23</sup> found that the tendency to form gas bubbles increased as the ambient pressure over the water was increased. Increasing the time of stirring prior to freezing increased the number of gas bubbles in aluminum A356 alloy.<sup>31</sup>

The freezing rate is another critical factor in bubble formation and trapping. Chernov et al.<sup>32,33</sup> experimentally demonstrated with water that bubble capture occurs when the growth rate exceeds a critical value that decreases as the bubble diameter increases. Bagdasarov et al.<sup>25</sup> developed a theory for this critical freezing rate. Bari and Hallett<sup>34</sup> observed the formation and growth of bubbles during freezing of water with air and helium dissolved in it. Cylindrical gas tubes formed in the ice when the freezing rate was below 0.005 mm/s. Egg-shaped bubbles were trapped when the freezing rate was higher. The number and the size of the bubbles decreased as the freezing rate increased. The same conclusion was reached by Carte.<sup>22</sup>

Convection also influences the concentration field of dissolved gas and, thereby, bubble nucleation and evolution. Thus, stirring decreased the tendency to form bubbles in ice.<sup>23</sup> Miyazawa<sup>35</sup> found that gas bubble entrapment during Czochralski growth of  $\text{Pb}_5\text{Ge}_3\text{O}_{11}$  and  $\text{TeO}_2$  single crystals could be avoided by making the interface shape flat or a little concave to the melt.

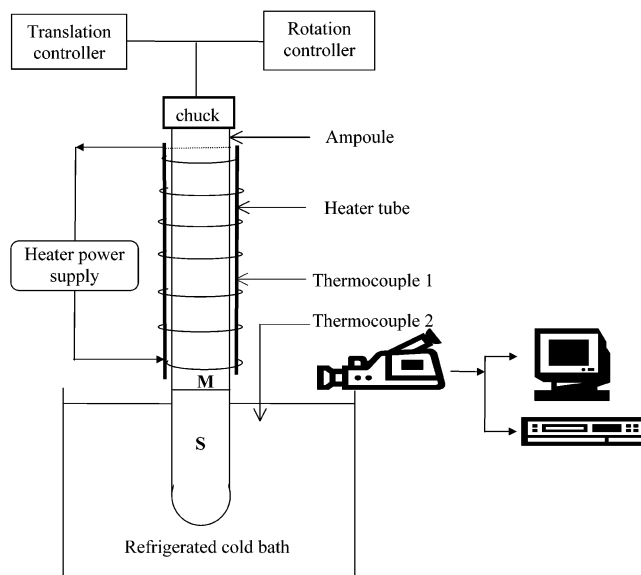


**Figure 1.** Experimental set up.

The interface shape depended primarily on crystal rotation rate and crystal diameter. Fukuda et al.<sup>36</sup> showed that formation of bubbles in  $\text{Ti:Al}_2\text{O}_3$  single crystals grown by the Czochralski method depended on the freezing interface shape, which varied with the rotation rate. When the interface was convex into the melt, gas tubes formed along the center of the crystal. As the freezing rate was lowered, the number of bubbles decreased (unlike the behavior in freezing water without stirring<sup>22,34</sup>).

Nucleation of gas bubbles can be influenced by other factors. For example, increasing the height of water over the freezing interface decreased bubble nucleation.<sup>23</sup> Air bubbles formed along a scratch on the freezing interface when the supersaturation was otherwise insufficient to form bubbles.<sup>37</sup>

Another interesting observation was that bubbles in ice tended to occur in layers perpendicular to the growth direction.<sup>26</sup> This was explained as follows. The growth of bubbles leads to a drop in supersaturation of the dissolved gas near the freezing interface, thereby stopping nucleation. Accumulation of dissolved gas near the interface begins anew after capture of the bubbles, until nucleation again occurs. An alternate explanation would be an oscillation in growth rate, with nucleation of bubbles occurring when the growth rate is increased.

Many other papers also have reported gas bubbles and tubes in ice (e.g., refs 38–42), but none dealing with bubbles and tubes on the ampoule wall as reported here.

## 2. Experimental Methods

The experiments are described in detail elsewhere.<sup>43</sup> A vertical Bridgman-Stockbarger apparatus was used to slowly freeze water. This apparatus allowed in-situ observation of the solid-liquid interface, formation and evolution of gas bubbles in the solid and liquid phases during solidification, and convection in the water. Figure 1 is a schematic diagram of the experimental set up. The apparatus consisted of a translation stage mounted vertically, a motor placed on the moving mount of the translation stage, a heater, a refrigerated bath, a CCD camera, a video monitor, and a time-lapse VCR. The motor had a vertical shaft with a chuck used to hold the top

of the ampoule. Thus, the ampoule could be translated vertically and rotated around its axis. Ampoule diameters of 5, 10, and 20 mm were used. Each ampoule's bottom end was closed, and its top end was open. The ampoules were approximately 30-cm long and were filled to about 12 cm with water. The heater was constructed by winding Nichrome wire around a quartz tube, with an inner diameter slightly larger than the outer diameter of the ampoule. The height of the heating section was about 8 cm and the maximum power was 250 W. Automotive antifreeze was used as a working liquid in the refrigerated bath.

To start an experiment, the ampoule containing the water was lowered so that the bottom was immersed 5 to 10 cm into the cold bath. It was adjusted so that it was vertical, as judged by its video image, which was very sensitive to misalignment. If no ice was observed after 30 min in the cold bath, the ampoule was shaken to induce nucleation. When the freezing interface came into view of the video camera above the surface of the cold bath, directional solidification was caused by slowly lowering the ampoule through the heater into the cold bath. Observations were begun after the ampoule had been lowered 2 to 3 cm, which was sufficient to reach steady state. The behavior of the solidification began to change when the freezing interface was within about 2 cm of the top surface of the water; the observations reported here are the steady-state behavior prior to this end effect. The temperatures of the heater and the cold bath were measured and displayed by type-K thermocouples and digital thermometers. In some experiments, the temperature was measured at the ice–water interface and at 2-mm intervals up to 20 mm above the interface. The temperature increased steadily with height, with a gradient of about 0.5 °C just above the freezing interface. Sometimes the ampoule was rotated slowly, up to 10 rpm, both to permit viewing of the entire periphery and to ensure thermal symmetry.

To increase the contact angle of water on the ampoule wall, the inside surface of some ampoules was coated with silicone oil,<sup>50</sup> Teflon, or Teflon with powder dispersed in it.<sup>20</sup> For uncoated and cleaned Pyrex the apparent contact angle was near 0°, after coating with silicone oil about 80°, with Teflon coating 121°, and for Teflon with powder 146°. Some of the coatings containing powder were sufficiently transparent to permit viewing of bubble behavior on the wall, while some were not. The other coatings were all transparent.

Different sources of water were used, including deionized, doubly distilled, and high-pressure liquid-chromatography water. Experiments were performed after bubbling either air or carbon dioxide through the water for at least 1 h.

A camera on a microscope was used to photograph the freezing interface and the ice before and after removal of the Pyrex tube, at a magnification of 1 to 7. After freezing, the ampoule was quickly taken out and a photograph was taken of the region near the interface. A small hammer was used to break off the glass, taking care not to disturb the outer surface of the ice. To show a cross section of the sample, the ice was carefully cut with a knife. Thereby both longitudinal and cross-sectional views were photographed.

A laser light-cut technique was used to observe convection in the water near the solid–liquid interface. Figure 2 shows the set up. A vertical sheet of laser light in the water was created with a glass rod placed horizontally in front of a laser beam. Very small guanine particles<sup>51</sup> were stirred in the water.

Particle-tracking velocimetry was used to measure particle velocities throughout the viewing field, for about 3 mm above the interface. Using a frame grabber and image analysis software, each particle's velocity was calculated from the distance it moved between frames divided by the time span.<sup>52</sup>

### 3. Experimental Results

In all of the experiments, the vertical position of the interface did not change noticeably during solidification, with translation rates from 0.4 to 100 mm/h. This indicates that the freezing rate was the same as the

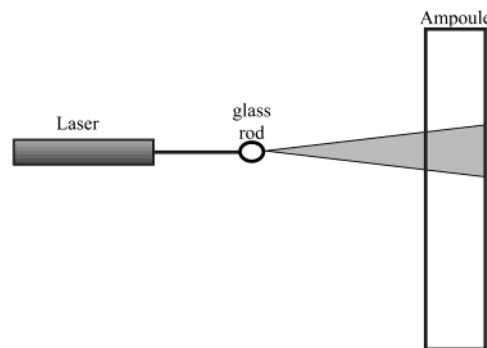


**Figure 2.** Laser light cut technique used to observe convection.

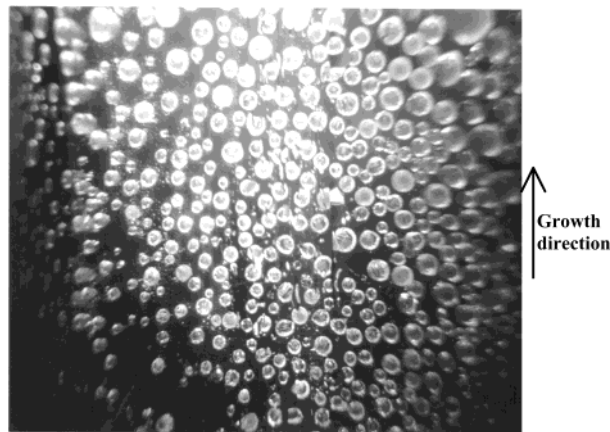


**Figure 3.** Gas bubbles formed on the ampoule wall during freezing with ampoule rotation. The water was saturated with air and the ampoule was coated with Teflon. Freezing rate 12 mm/h, cooling bath  $-20$  °C, heater 40 °C, ampoule rotated at 1.5 rpm, ampoule inside diameter 10 mm. The width of the sample shown above is about 8.5 cm.

translation rate. During solidification, gas bubbles often formed on the interface. (Gas bubble formation was never observed in the bulk water.) Some bubbles broke free of the freezing interface and rose quickly to escape, while others were captured by the interface as isolated bubbles or grew with the moving interface to form gas tubes. A few experiments were repeated and gave the same behavior.

**3.1. Gas Bubbles and Tubes on the Ampoule Wall.** Operating conditions influencing bubble formation and behavior included freezing rate, heater and refrigerated bath temperatures, the identity of the gas dissolved in the water, and the contact angle of the water on the ampoule wall. Under some operating conditions, gas bubbles or tubes formed and were incorporated in the ice only at the ampoule wall, and not in the interior. Results did not depend on the source or type of water used. Three kinds of regular bubbles formed on the wall:

**Isolated Gas Bubbles.** Under some conditions, bubbles forming around the ampoule wall were captured by the interface and stayed in the solid. Figure 3 is a photograph taken after such an experiment. These isolated bubbles were nearly uniformly distributed along the ampoule wall.

**Long and Narrow Cylindrical Gas Tubes.** Under other conditions, the bubbles grew as the interface moved along the ampoule wall to form long gas tubes.

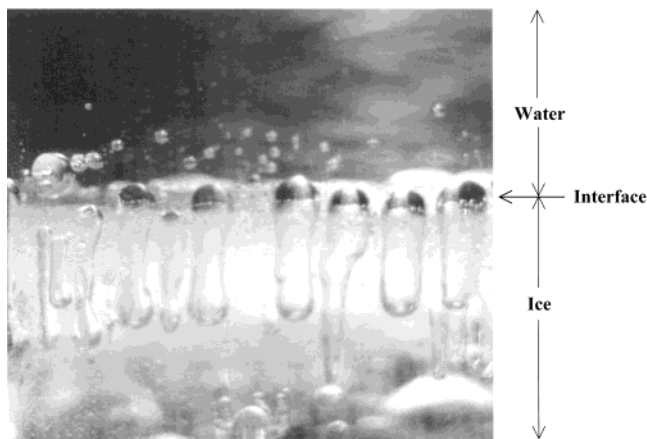


**Figure 4.** Gas tubes forming on the ampoule wall during freezing. The water was saturated with air, the ampoule was coated with Teflon, freezing rate 20 mm/h, cold bath temperature  $-20\text{ }^{\circ}\text{C}$ , heater temperature  $40\text{ }^{\circ}\text{C}$ , no ampoule rotation, ampoule inside diameter 10 mm. Width of the sample shown is about 4 cm.

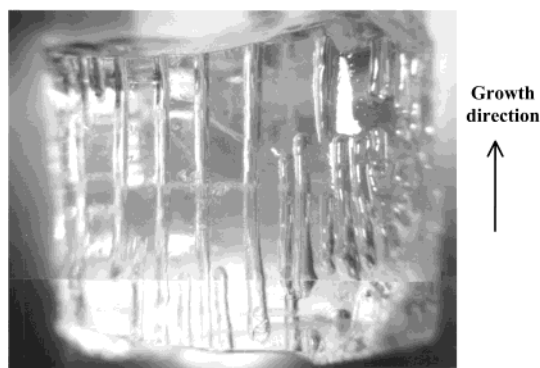


**Figure 5.** Gas tubes on the ampoule wall after freezing. Composite of two photographs taken after removal of the ampoule. The water was saturated with air and the ampoule was coated with Teflon. Freezing rate 12 mm/h, cooling bath  $-20\text{ }^{\circ}\text{C}$ , heater  $40\text{ }^{\circ}\text{C}$ , no ampoule rotation, ampoule inside diameter 10 mm. Width shown above is 10 mm.

(Similar results were obtained with naphthalene.<sup>20</sup>) Figure 4 is an example during freezing at 12 mm/h,  $-20\text{ }^{\circ}\text{C}$  cooling bath,  $40\text{ }^{\circ}\text{C}$  heater, and no ampoule rotation. The almost-flat freezing interface can be seen. The spherical portion of the gas tube above the interface moved with the interface, so that a long, nearly cylindrical, gas tube formed. Figure 5 was taken after freezing and shows a longitudinal section with gas tubes distributed fairly regularly on the outer surface of the sample. As discussed later, the occurrence of such behavior seemed to depend on the rotation rate, the freezing rate, the contact angle, and the temperature settings, with the rotation rate being the main factor affecting the transformation of gas bubbles to gas tubes. Figure 6 is a cross-section of the sample shown in Figure 4. The notches distributed around the periphery of the sample show the positions and the nearly semi-cylindrical shapes of the gas tubes. Along the edge of the notch, the contact angle on the ampoule wall was measured as around  $120^{\circ}$ , which is almost the same as that measured for a water drop on a coated microscope slide.<sup>20</sup> Such periodic gas tubes seem not to have been reported before. The fraction of the ice surface thereby

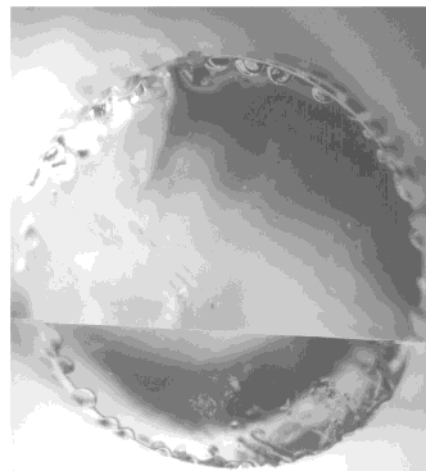


**Figure 6.** End view of a cross section of the sample shown in Figure 4. Composite of two photographs taken after removal of the ampoule. The water was saturated with air and the ampoule was coated with Teflon. Freezing rate 20 mm/h, cooling bath  $-20\text{ }^{\circ}\text{C}$ , heater  $40\text{ }^{\circ}\text{C}$ , no rotation, ampoule inside diameter 10 mm. Diameter of sample shown is 10 mm.

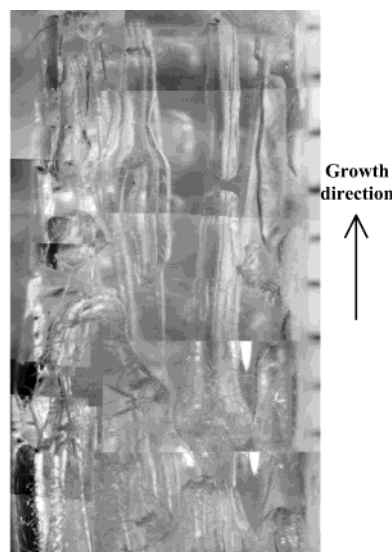


**Figure 7.** Larger gas tubes on the ampoule wall with  $\text{CO}_2$  dissolved in the water. Composite formed of several photographs taken after removal of the ampoule. The water was saturated with  $\text{CO}_2$  and the ampoule was coated with Teflon. Freezing rate 20 mm/h, cooling bath  $-20\text{ }^{\circ}\text{C}$ , heater  $40\text{ }^{\circ}\text{C}$ , no rotation, ampoule inside diameter 10 mm. The width of the sample is 10 mm.

detached from the ampoule wall is estimated to have been about 60%.

**Wide Gas Tubes.** As shown in Figure 7, some gas tubes grew so wide that adjacent tubes merged to form a larger tube. The most important parameters affecting the sizes of gas tubes was the amount of gas dissolved in the water, as discussed later.

Although 95% detachment was achieved with a rough nonwetting coating on the ampoule wall, under no condition did bubbles or tubes propagate around the wall to yield fully detached solidification.

**3.2. Influence of the Contact Angle.** The influence of the contact angle on the formation and behavior of gas bubbles can be seen in Figures 5, 8, and 9. Figures 8 and 9 are with an uncoated cleaned ampoule. Figure

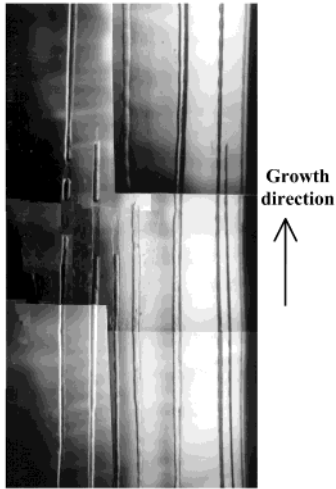


**Figure 8.** Gas tubes formed on the ampoule wall. Composite of several photographs taken after removal of the ampoule. The water was saturated with air and the ampoule was uncoated. Freezing rate 12 mm/h, cooling bath  $-20\text{ }^{\circ}\text{C}$ , heater  $40\text{ }^{\circ}\text{C}$ , no rotation, ampoule inside diameter 10 mm. Sample width 10 mm.

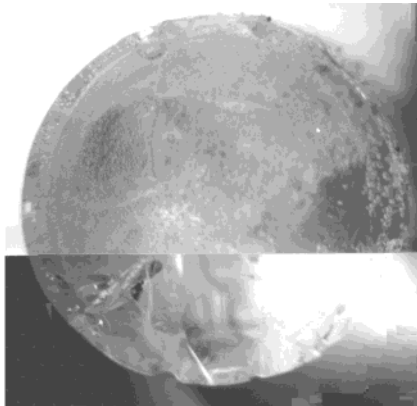


**Figure 9.** Cross section of the sample shown in Figure 8.

5 is for an ampoule coated with Teflon, with the other conditions being the same as Figure 8. Note that the number of gas tubes in Figure 6 is much more than in Figure 9.

**3.3. Influence of the Freezing Rate.** No gas bubble or tube formed in the interior or on the ampoule wall if the freezing rate was below a value that depended on the ampoule diameter, temperature settings, rotation rate, and the dissolved gas. When the freezing rate was above another higher level, gas bubbles and tubes appeared not only on the ampoule wall but also in the interior. When the freezing rate was between these two values, all gas bubbles appeared on the ampoule wall as discrete bubbles or grew along the ampoule wall to form tubes. When gas tubes formed, they were distributed fairly regularly around the periphery of the ampoule wall. The number of gas tubes around the ampoule wall was counted, so that the average periodicity could be calculated. The period decreased as the freezing rate was increased, as shown in Figures 10 and 11 (these two photographs were taken at the same magnification). The quantitative relationship between period and freezing rate is given in the next section.

**3.4. Influence of the Ampoule Diameter.** Gas bubbles or periodic tubes formed on the ampoule wall

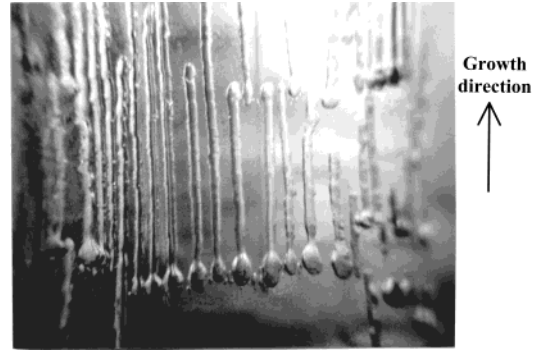


**Figure 10.** Gas tubes on the surface of the ampoule. The water was saturated with air and the ampoule was coated with Teflon. Freezing rate 20 mm/h, cooling bath  $-20\text{ }^{\circ}\text{C}$ , heater  $40\text{ }^{\circ}\text{C}$ , no rotation, ampoule inside diameter 10 mm. Sample width  $\sim 10\text{ mm}$ .

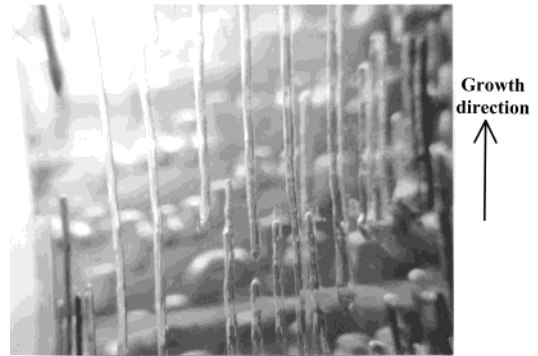


**Figure 11.** Influence of freezing rate on gas tube width and spacing. Freezing rate 12 mm/h with the other conditions the same as Figure 10. Sample width  $\sim 10\text{ cm}$ .

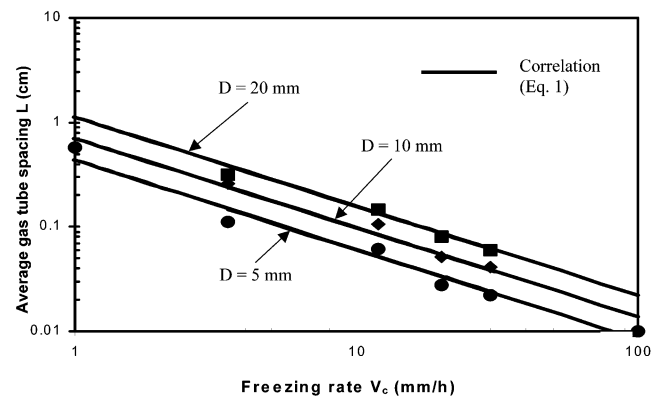


**Figure 12.** Average spacing of gas tubes versus freezing rate and ampoule diameter. The water was saturated with air and the ampoule was coated with Teflon, cooling bath  $-20\text{ }^{\circ}\text{C}$ , heater  $40\text{ }^{\circ}\text{C}$ , no rotation. Squares for 20-mm diameter ampoules, diamonds 20 mm, and circles 5 mm.

under proper operating conditions for all three ampoule diameters. Increasing the ampoule diameter increased the spacing between gas tubes. Figure 12 shows the dependence of the average spacing  $L$  between gas tubes on freezing rate  $V_c$  and ampoule diameter  $D$ .

Linear regression analysis of the logarithms of  $L$ ,  $D$ , and  $V_c$  gave:

$$L = 0.142D^{0.69}V_c^{-0.85} \quad (1)$$

with a correlation coefficient  $R$  of 0.95. The width of the

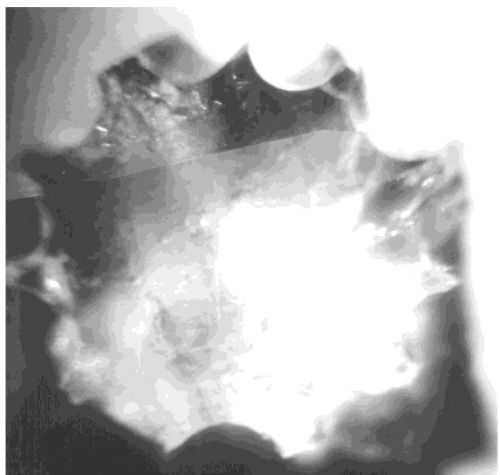


**Figure 13.** Cross section of the sample shown in Figure 7.

gas tubes was about  $0.65 \pm 0.03$  mm, nearly independent of freezing rate and ampoule diameter.

**3.5. Influence of Gas Dissolved in Water.** At 1 atm and 0 °C, the solubilities of O<sub>2</sub>, N<sub>2</sub>, and CO<sub>2</sub> in water are, respectively,  $2.8 \times 10^{-5}$ ,  $1.4 \times 10^{-5}$ , and  $1.3 \times 10^{-3}$  mole fraction.<sup>44</sup> Thus, the solubility of air in water is much less than that of CO<sub>2</sub> at the same temperature and partial pressure. Figure 7 shows the result of an experiment for water initially saturated with CO<sub>2</sub> at 1 atm. Figure 13 is a cross section of this sample. The fraction of detachment is estimated to have been 85%. Figure 6 shows an experiment for water initially saturated with air at 1 atm.

During the two experiments shown in Figures 6 and 7, the operating conditions were carefully kept the same, except for the gas dissolved. The interface shape and convection pattern were the same. The gas bubbles and tubes were much larger when CO<sub>2</sub> was used. The width of air gas tube in Figure 6 is about 0.7 mm, while the width of the CO<sub>2</sub>-containing gas tube in Figure 7 is about 2.5 mm.

**3.6. Influence of Heater Temperature.** When all of the other operating parameters were held constant, if the temperature of the heater was below a critical level, many gas bubbles and tubes were trapped both in the interior and on the ampoule wall. If the heater temperature was above a higher critical value, no bubbles or tubes were trapped anywhere in the ice. Between these critical values, bubbles and tubes were trapped at the ampoule wall and not in the interior. As discussed later, the heater temperature influences the interface shape and the convection in the melt.

**3.7. Influence of Rotation of the Ampoule.** When the ampoule was rotated about its axis, gas bubbles and tubes were seldom observed, as shown in Figure 3. With the other conditions the same as in Figure 3, long cylindrical gas tubes were observed when the ampoule was not rotated (see Figure 5).

**3.8. Influence of Rough Teflon Coating.** The presence of rough particles in the Teflon coating not only increased the contact angle but also influenced the behavior of the gas bubbles and tubes. During freezing, many small gas bubbles nucleated at particles at the wall near the interface.<sup>53</sup> When a gas tube grew near such small gas bubbles, it absorbed them and became irregular, as shown in Figure 14. Figure 15 is a

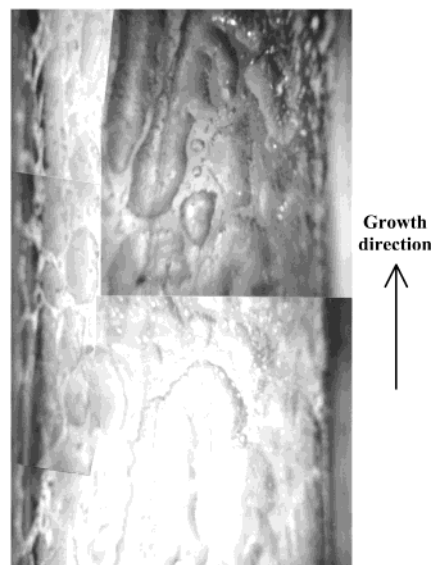


**Figure 14.** Surface of ice frozen in an ampoule that had been coated with Teflon containing a powder. Composite of several photographs taken after the ampoule had been removed. The water was saturated with air. Freezing rate 12 mm/h, cooling bath -20 °C, heater 40 °C, no rotation, ampoule inside diameter 10 mm. Width of sample shown 10 mm.



**Figure 15.** Cross section of the sample shown in Figure 14.

photograph of a cross section from an experiment with a powder-containing coating. The periphery was very irregular and the fraction detached was about 95%.

**3.9. Freezing Interface Shape and Convection.** The temperature settings and the freezing rate determined the shape of the freezing interface and the convection in the adjacent melt. In 10- and 20-mm diameter ampoules an unexpected relationship was observed between heater temperature, convection pattern, and interface shape. Figure 16 shows an example of the influence of the heater temperature on the interface shape and convection intensity, with the temperature of the cold bath at -20 °C. When the temperature of the heater was 20 °C, the interface was convex, there were two axisymmetric counter-rotating vortices in the water, and the flow near the interface

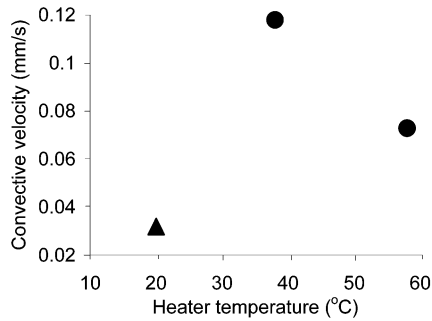


**Figure 16.** Convective velocity versus heater temperature. The water was saturated with air and the ampoule was coated with Teflon. Freezing rate 12 mm/h, cooling bath  $-20\text{ }^{\circ}\text{C}$ , no rotation, ampoule inside diameter 10 mm. The circles are for a concave freezing interface and the triangle for a convex interface (curved into the melt).

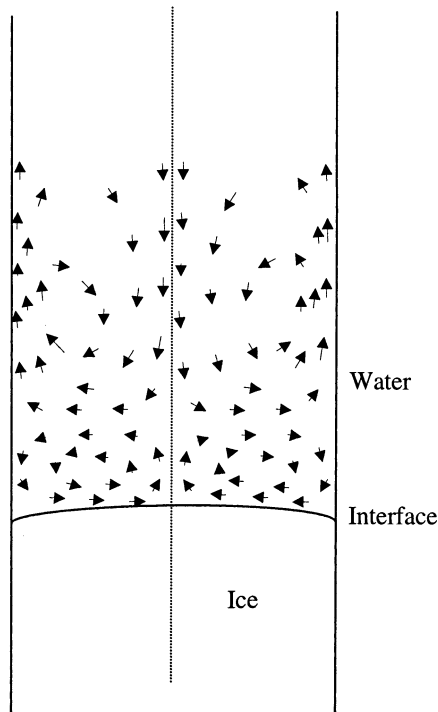


**Figure 17.** Convection with a slightly convex freezing interface. The water was saturated with air and the ampoule was coated with Teflon. Freezing rate 12 mm/h, cooling bath  $-20\text{ }^{\circ}\text{C}$ , heater  $20\text{ }^{\circ}\text{C}$ , no ampoule rotation, ampoule inside diameter 10 mm.

was from the periphery toward the center, as shown in Figure 17. When the temperature of the heater was increased to  $40\text{ }^{\circ}\text{C}$ , the interface became nearly flat, there were two axisymmetric counter-rotating vortices, and the flow near the freezing interface was from the center toward the periphery, as shown in Figure 18. When the temperature of the heater was increased to  $60\text{ }^{\circ}\text{C}$ , the interface became more concave, the lower vortex became larger and the upper vortex nearly disappeared, as shown in Figure 19. In all prior literature, both experimental and theoretical, the flow near a freezing interface has been found to be inward for a concave interface and outward for a convex interface (e.g., refs 45–48). The reverse behavior observed here is attributed to the maximum density of water at  $4\text{ }^{\circ}\text{C}$ . With an estimated vertical temperature gradient of  $0.5\text{ }^{\circ}\text{C}/\text{mm}$ , there was a density inversion up to about 8 mm,

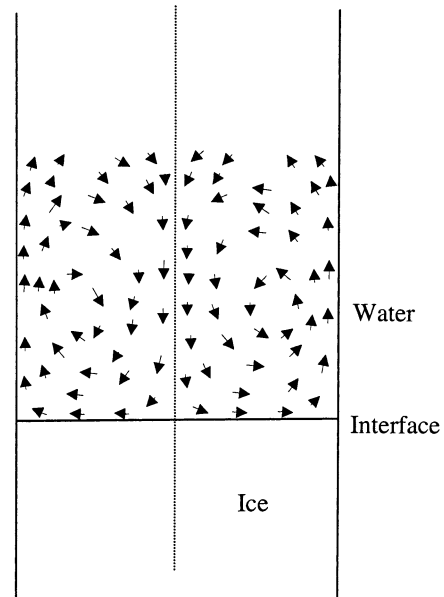


**Figure 18.** Convection with a very slightly concave freezing interface. The water was saturated with air and the ampoule was coated with Teflon. Freezing rate 12 mm/h, cooling bath  $-20\text{ }^{\circ}\text{C}$ , heater  $40\text{ }^{\circ}\text{C}$ , no rotation, ampoule inside diameter 10 mm.

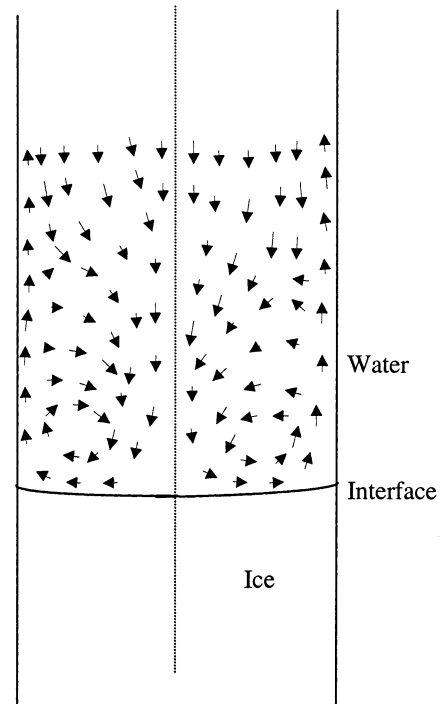


**Figure 19.** Convection with a concave freezing interface. The water was saturated with air and the ampoule was coated with Teflon. Freezing rate 12 mm/h, cooling bath  $-20\text{ }^{\circ}\text{C}$ , heater  $60\text{ }^{\circ}\text{C}$ , no rotation, ampoule inside diameter 10 mm.

which is more than sufficient to strongly influence convection. Figure 20 shows the influence of the freezing rate on the convection velocity. In the 5-mm diameter ampoule, we observed only a single asymmetric vortex. The flow was always upward on the side illuminated by the laser, indicating that heating by the laser was the cause of the asymmetry. It is interesting that this heating was insufficient to alter the pattern in the larger diameter ampoules.

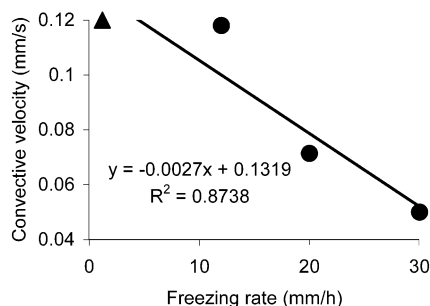


**Figure 20.** Convective velocity versus freezing rate. The water was saturated with air and the ampoule was coated with Teflon, ampoule inside diameter 10 mm, cooling bath  $-20^{\circ}\text{C}$ , heater  $40^{\circ}\text{C}$ , no ampoule rotation. The circles are for concave freezing interfaces (at 12 mm/h, only very slightly so), while the triangle is for a convex interface.

#### 4. Discussion and Conclusions

Gas bubbles and tubes at the ampoule wall did not propagate around the periphery of the freezing interface, so we must rule this out as a likely mechanism for initiation of detached solidification. Thus, spontaneous detachment of high-melting materials probably occurred because the stress caused by thermal contraction became sufficient to overcome adhesion. Why did this not occur in ice (or naphthalene<sup>20</sup>)? We believe this was because these materials more readily plastically deform, so that they did not pop free of the ampoule, at least at the freezing interface. Furthermore, their melting points are lower so that they undergo much less cooling from the temperature at the freezing interface. Nevertheless, several interesting phenomena were observed in the course of the present experiments, including a high degree of detachment when a high-solubility gas ( $\text{CO}_2$ ) was dissolved in the water together with a rough, nonwetting coating on the ampoule wall.

Under proper operating conditions, isolated gas bubbles, long gas tubes or wide gas tubes grew on the ampoule wall and not in the interior. Within the range of freezing rates where gas tubes formed on the ampoule wall, eq 1 shows that decreasing the freezing rate and increasing the ampoule diameter increased the average spacing between gas tubes. Let us attempt to rationalize this observation. In the absence of convection, the diffusion length is proportional to the square root of the time available, or to  $1/\sqrt{V_C}$ . If the spacing were proportional to the diffusion length, we would predict an exponent of  $-1/2$  on  $V_C$ , and  $-1$  if the spacing goes as the diffusion area (i.e., length squared). The actual exponent lies between these. The increase of spacing with tube diameter may indicate an influence of convection, which should increase in intensity with increasing diameter. Increasing convection increases the portion of the freezing interface from which the propagating gas tube can collect dissolved gas rejected by the interface.

Note also that the freezing rate influences both the interface shape and the transport of dissolved gas in the water near the freezing interface. Increasing the freezing rate increases the segregation of dissolved gas by the freezing interface, making it more likely for gas bubble nucleation and growth to occur there. Increasing

the freezing rate also causes the interface to move downward and become less convex, thereby changing the convection. When the freezing rate was low, the interface and convection were as shown in Figure 17. When the water near the interface flowed from the periphery toward the center, this convection prevented the segregated gas from accumulating around the ampoule wall. When the freezing rate was increased, the interface and convection were as shown in Figures 18 and 19. This mode of convection would enhance the transport of the segregated gas outward to the wall and favor the growth of gas bubbles there, provided that it is not so vigorous as to remove segregated gas from the neighborhood of the interface.

Ampoules of 10- and 20-mm inside diameter showed the same convection pattern (Figures 17, 18, and 19). We attribute the different convection pattern in the 5-mm diameter to preferential heating of one side of system by the laser used to illuminate it.

There was an optimal heater temperature range for the formation and growth of gas bubbles on the ampoule wall. When the temperatures of the cold bath was kept constant, the heater and cooler temperature influenced interface position, shape, and convection. When the temperature of the heater was low, the concentration of the dissolved gas in the water was high and the convection was as shown in Figure 17. Then bubbles nucleated everywhere. When the temperature of the heater was high and the convection was as shown in Figure 19, the amount of gas dissolved in the melt was insufficient to nucleate bubbles.

Slow rotation diminished the transformation of gas bubbles to tubes. Rotation of the ampoule, even at these low rates, was apparently sufficient to alter the convective transport of dissolved gas from the freezing interface outward to the wall, thus preventing gas bubbles from becoming tubes. It has been observed that the Coriolis force strongly deflects flow in the Bridgman technique, even at low rotation rates.<sup>49</sup>

**Acknowledgment.** This research was supported by NASA under Grant NAG 8-1482. We thank Peter Skudarnov for helping to set up the initial experimental apparatus.

#### References

- (1) Regel, L. L.; Wilcox, W. R. *Microgravity Sci. Technol.* **1999**, *14*, 152–166.
- (2) Duffar, T.; Dusserre, P.; Picca, F.; Lacroix, S.; Giacometti, N. *J. Cryst. Growth* **2000**, *211*, 434–440.
- (3) Duffar, T.; Dusserre, P.; Giacometti, N. *J. Cryst. Growth* **2001**, *223*, 69–72.
- (4) Dold, P.; Szofran, F. R.; Benz, K. W. *J. Cryst. Growth* **2002**, *234*, 91–98.
- (5) Schweizer, M.; Volz, M. P.; Cobb, S. D.; Vujisic, L.; Motakef, S.; Szoke, J.; Szofran, F. R. Stability of Detached-Grown Germanium Single Crystals. International Conference on Crystal Growth 13, Kyoto, Japan, 2001.
- (6) Volz, M. P.; Schweizer, M.; Kaiser, N.; Cobb, S. D.; Vujisic, L.; Motakef, S.; Szofran, F. R. Bridgman Growth of Detached GeSi Crystals. International Conference on Crystal Growth 13, Kyoto, Japan, 2001.
- (7) Schweizer, M.; Cobb, S. D.; Volz, M. P.; Szoke, J.; Szofran, F. R. Defect Density Comparison of Detached versus Attached Bridgman-grown Germanium Crystals. At Thir-

- teenth American Conference on Crystal Growth & Epitaxy, 2001, Burlington, Vermont.
- (8) Dold, P.; Kaiser, N.; Benz, K. W.; Cröll, A.; Szofran, F. R.; Cobb, S.; Volz, M.; Schweizer, M. "RDGS" (Reduction of Defects in Germanium-Silicon) Detached and Floating-Zone Growth of Semiconductor Crystals on the ISS. 51st International Astronautical Congress, 2000, Rio de Janeiro, Brazil.
- (9) Wang, J. *Detached Solidification of Indium Antimonide in Pyrolytic Boron Nitride*, M.S. Thesis, Clarkson University, Potsdam, NY, 2002.
- (10) Wilcox, W. R.; Regel, L. L. *Microgravity Sci. Technol.* **1995**, *8*, 56–61.
- (11) Popov, D. I.; Regel, L. L.; Wilcox, W. R. *J. Mater. Synth., Proc.* **1997**, *5*, 283–297.
- (12) Popov, D. I.; Regel, L. L.; Wilcox, W. R. *J. Mater. Synth., Proc.* **1997**, *5*, 299–311.
- (13) Popov, D. I.; Regel, L. L.; Wilcox, W. R. *J. Mater. Synth., Proc.* **1997**, *5*, 313–336.
- (14) Wang, Y.; Regel, L. L.; Wilcox, W. R. *J. Cryst. Growth* **2000**, *209*, 175–180.
- (15) Wang, Y.; Regel, L. L.; Wilcox, W. R. *J. Cryst. Growth* **2001**, *226*, 430–435.
- (16) Wang, Y.; Regel, L. L.; Wilcox, W. R. Approximate Material Balance Solution to the Moving Meniscus Model of Detached Solidification, *J. Cryst. Growth*, submitted.
- (17) Regel, L. L.; Wilcox, W. R. Detached Solidification. In *Proceedings of the First Pan Pacific Basin Workshop on Microgravity Sciences*, *J. Jpn. Soc. Microgravity Appl.* **1998**, *15*, 460–465.
- (18) Regel, L. L.; Wilcox, W. R. Improved Crystal Quality by Detached Solidification in Microgravity. In *Proceedings of the 1998 Microgravity Materials Science Conference*, compiled by Gillies, D. C., and McCauley, D. E., NASA/CP-1999-209092, Marshall Space Flight Center, 1999; pp 533–540.
- (19) Regel, L. L.; Wilcox, W. R.; Wang, Y.; Burkhard, C. Improved Crystal Quality by Detached Solidification in Microgravity. In *Proceedings of the Microgravity Materials Science Conference 2000*, Ramachandran, N., Bennett, N., McCauley, D., Murphy, K., Poindexter, S., Eds.; NASA/CP-2001-210827, 2001; pp 487–492.
- (20) Burkhard, C. *Solidification of Zone-Refined Naphthalene and High Contact Angle Coatings*, M.S. Thesis, Clarkson University, Potsdam, New York, 2002.
- (21) Wilcox, W. R.; Kuo, V. H. S. *J. Cryst. Growth* **1973**, *19*, 221–228.
- (22) Carte, A. E. *Proc. Phys. Soc.* **1961**, *77*, 758–766.
- (23) Vasconcellos, K. F.; Beech, J. *J. Cryst. Growth* **1975**, *28*, 85–92.
- (24) Cole, R.; Papazian, J. M.; Wilcox, W. R. *Int. J. Heat Mass Transfer* **1980**, *23*, 219–224.
- (25) Bagdasarov, K. H. S.; Okinshevich, V. V.; Kholov, A. *Phys. Stat. Sol. (a)* **1980**, *58*, 317.
- (26) Geguzin, Y. I.; Dzyuba, A. S. *J. Cryst. Growth* **1991**, *110*, 101–111.
- (27) Maeno, N. In *Proceedings of the International Conference on Low-Temperature Science, Physics of Snow and Ice* **1966**, *1*, 207–217.
- (28) Akamatsu, S.; Faivre, G. *J. Phys. France* **1995**, *65*, 99–105.
- (29) Brunner, C. *Ann. Phys.* **1845**, *64*, 113.
- (30) Bunsen, R. *Ann. Phys.* **1870**, *141*, 1.
- (31) Serratos, M.; Poirier, D. R., private communication, University of Arizona, Tucson, 2000.
- (32) Chernov, A. A.; Temkin, D. E.; Melnikova, A. M. *Kristallografiya* **1977**, *22*, 27.
- (33) Chernov, A. A.; Temkin, D. E.; Melnikova, A. M. *Kristallografiya* **1977**, *22*, 1152.
- (34) Bari, S. A.; Hallett, J. *J. Glaciology* **1974**, *13*, 489–519.
- (35) Miyazawa, S. *J. Cryst. Growth* **1980**, *49*, 515–521.
- (36) Neftel, A.; Okanao, Y.; Kodama, N. *Cryst. Res. Technol.* **1995**, *30*, 185–188.
- (37) Maeno, N. In *Physics of Snow and Ice*, Vol. I, Part 1, Oura, H., Ed.; Hokkaido University, Sapporo, Japan, 1967; p 207.
- (38) Neftel, A.; Oeschger, H.; Schwander, J.; Stauffer, B. *J. Phys. Chem.* **1983**, *87*, 4116–4120.
- (39) Gary, K. *Appl. Optics* **1987**, *26*, 5143–5147.
- (40) Vesenska, J. P.; Yeh, Y. *Phys. Rev. A: Gen. Phys.* **1988**, *38*, 5310–5315.
- (41) Frank, P.; Josef, K.; Werner, W. F. *Geophys. Res. Lett.* **1996**, *23*, 177–180.
- (42) Drzymala, J.; Sadowski, Z.; Holysz, L.; Chibowski, E. *J. Colloid Interface Sci.* **1999**, *220*, 229–234.
- (43) Wang, Y. *Modeling and Ground-Based Experiments on Detached Solidification*, Ph.D. Dissertation, Clarkson University, Potsdam, New York, 2001.
- (44) Lide, D. R., Ed., *Handbook of Chemistry and Physics*, 76th ed.; Chemical Rubber Publishing Company, Boca Raton, FL, 1995–1996.
- (45) Neugebauer, G. T.; Wilcox, W. R. *J. Cryst. Growth* **1988**, *89*, 143–154.
- (46) Neugebauer, G. T.; Wilcox, W. R. *Acta Astron.* **1991**, *25*, 357–362.
- (47) Müller, G.; Neumann, G.; Weber, W. *J. Cryst. Growth* **1984**, *70*, 78–93.
- (48) Carlson, F. M.; Fripp, A. L.; Crouch, R. K. *J. Cryst. Growth* **1984**, *68*, 747–756.
- (49) Skudarnov, P. V.; Regel, L. L.; Wilcox, W. R.; Ahmadi, G. Numerical Modeling and Flow Visualization in the Gradient Freeze Configuration during Centrifugation, In *Processing by Centrifugation*; Regel, L. L., Wilcox, W. R., Eds.; Kluwer Academic/Plenum: New York, 2001; pp 273–286.
- (50) SF96-100, from General Electric Company, Waterford, NY 12188.
- (51) Guanine 99+%, from Acros Organics, NJ 07960.
- (52) HLIImage ++ 98, Western Vision Software, Salt Lake City, UT 84111.
- (53) As seen in those ampoules with a semi-transparent rough coating.

CG0255063